Waste Management 168 (2023) 431–439

Contents lists available at ScienceDirect

Waste Management

journal homepage: www.elsevier.com/locate/wasman

Research Paper

Dolomite industrial by-products as active material for CO_2 adsorption and catalyst for the acetone condensation

David Ursueguía [a], Laura Faba [a], Eva Díaz [a], Roberto Caballero [b], Salvador Ordóñez [a,*]

[a] Catalysis, Reactors and Control Research Group (CRC), Dept. of Chemical and Environmental Engineering. University of Oviedo, Julián Clavería s/n, Oviedo 33006, Spain

[b] Intocast Ibérica, Av. Conde Santa Bárbara, 12, Lugones 33420, Spain

ARTICLE INFO

Keywords:
Refractory industry by-products
CO_2-capture
Aldol condensation
Base-catalysts
Alkaline wastes

ABSTRACT

The feasibility of using dolomite powders, by-product from the refractory industry, as a CO_2 adsorbent and as a catalyst for the acetone liquid-phase self-condensation is demonstrated in this article. The performance of this material can be largely improved by combining physical pretreatments (hydrothermal ageing, sonication) and thermal activation at different temperatures (500–800 °C). The highest CO_2 adsorption capacity was observed for the sample after sonication and activated at 500 °C (46 $mg \cdot g^{-1}$). As to the acetone condensation, the best results were obtained also with the sonicated dolomites, mainly after activation at 800 °C (17.4 % of conversion after 5 h at 120 °C). The kinetic model reveals that this material optimizes the equilibrium between catalytic activity (proportional to the total basicity) and deactivation by water (specific adsorption process). These results demonstrate that the valorisation of dolomite fines is feasible, proposing attractive pretreatments for obtaining activated materials with promising results as adsorbents and basic catalysts.

1. Introduction

Refractory materials (combinations of six basic oxides: MgO, CaO, SiO_2, Al_2O_3, Cr_2O_3 and ZrO_2) are needed in a plethora of industrial activities. Because of their high thermal (greater than1500 °C), chemical and mechanical resistance, these materials separate the reaction zone from the delicate outer parts of different devices. Thus, they are crucial to produce steel, iron, aluminium, glass, ceramics, and cement, among others key industrial sectors [Aksel'rod and Kvyatkovskii, 2003; Deneen et al., 2010; Muñoz et al., 2020].

Dolomite is a sedimentary rock enriched in the mineral of the same name (a calcium-magnesium carbonate, $CaMg(CO_3)_2$), with some impurities such as SiO_2, Al_2O_3 and Fe_2O_3. Dolomite is highly used in the production of refractory materials for steel making processes, with unbeatable properties as furnace wall coatings [Umadevi et al., 2009]. In addition, its chemical properties (basicity) increase the stability of the materials, mainly removing acids and sulphur, among other impurities [Duchesne and Reardon, 1999; Tian et al., 2019]. This material is also an excellent additive used in the glass sector, improving the durability of the final product by increasing its chemical stability and mechanical resistance, whereas it reduces the costs of its production by decreasing the melting point of the glass [Efremenkov, 2016]. In the same way, dolomite is also added to ceramic materials to increase the pore size of the final products, improving their applications as catalytic supports, thermal isolation, and filtration agents, among others [Qi et al., 2019].

The use of dolomite rocks in all these applications requires a thermal sintering to obtain the active CaO and MgO oxides [Ghosh and Tripathi, 2012], as well as a mechanical pretreatment to obtain the desired mechanical conformation, producing fines (<0.16 mm) that are rejected for the industrial processes. These fines have a highly hygroscopic character, and its surface is easily altered reaction with atmospheric water and CO_2, yielding a by-product difficult to upgrade. Currently, these fines are managed together with the dolomite by-products, representing a total amount of 20 million tons yearly [Seifert et al., 2021]. Since both by-products are considered together, their recycling potential and material valorisation is strongly limited by the poor properties of the exhausted material (volumetric instability, chemical contamination, structural damage). Thus, their reusability rate is lower than 10% and the final disposal in specific landfill is the main alternative [Muñoz et al., 2020, Furlani et al., 2021]. The development of recycling alternatives for these fines is a good opportunity for the harnessing of these streams, and to reduce the volume of wastes generated in the refractory industry.

Several researchers have studied the use of dolomitic materials for different applications in the field of the adsorption and catalysis. Thus,

* Corresponding author.
E-mail address: sordonez@uniovi.es (S. Ordóñez).

https://doi.org/10.1016/j.wasman.2023.06.031
Received 2 January 2023; Received in revised form 18 April 2023; Accepted 24 June 2023
Available online 28 June 2023

dolomite powder was tested as adsorbent of many heavy metals, obtaining capacities from 4 $mg{\cdot}g^{-1}$ to 20 $mg{\cdot}g^{-1}$, for Cd^{2+} and Pb^{2+}, respectively [Pehlivan et al., 2009; Ghaemi et al., 2011; Ghaemi et al., 2013]. These values, far from those reported with typical adsorbents such as active carbon [Serafin et al., 2021], are obtained in acidic conditions (pH 3 – 6), conditions at which the dolomite is not stable [Pehlivan et al., 2009]. A better behaviour as adsorbent is reported considering other water pollutants, such as phosphates (50 $mg{\cdot}g^{-1}$) [Karaca et al., 2006; Huang et al., 2018] or organic inks (up to 126 $mg{\cdot}g^{-1}$) [Yan et al., 2019].

The low specific surface area of this dolomite (~3 $m^2{\cdot}g^{-1}$) [Deng et al., 2022] justifies these weak results. Thus, different pretreatments were evaluated, including thermal activation [Yang et al., 2019a], hydration [Wang et al., 2015], or wet-ball milling [Sun et al., 2018], among others. These treatments increase the porosity and surface area, obtaining improved CaO/MgO distributions and structural defects. Thus, improved materials based on dolomites were tested as CO_2 adsorbent, obtaining significant retention capacities [Yang et al., 2019], and as a catalyst in different reactions, such as fatty-acids transesterification [Niu et al., 2014; Korkut et al., 2016], tar gasification [Rapagna et al., 2018; Meng et al., 2019; Islam 2020], deoxygenations [Hafriz et al., 2021] and Knoevenagel reactions [Tamaddon et al., 2013; Yang et al., 2019b].

These facts lead us to consider that these dolomitic by-products can be activated for their use both in CO_2 capture and as basic catalysts. At this last point, acetone self-condensation is an interesting model reaction for basic catalysts, because of the great industrial importance of mesityl oxide to produce green solvents (isophorones, mesitylene, among others) and fine chemistry intermediates. Last data available indicate a global market of mesityl oxide as final product higher than 11.7 USD million, being also the intermediate of methyl isobutyl ketone (MIBK), a very versatile solvent with a worldwide market calculated in 1080 USD million [Industry Research Biz, 2022].

A promising activity of these dolomitic materials could imply a significant reduction in the costs of the process, considering the complexity of the catalysts typically proposed in the literature (different oxides and mixed oxides with acidic/basic pairs that require specific manufacturing processes, including calcination, sintering, chemical decomposition and purification) [Al-Hazmi et al., 2013; Manriquez-Ramirez et al., 2020; Faba et al., 2021]. In addition to analyse its activity as received (the fines are produced after similar procedures, a specific process would be not required), in this work, we proposed the activation of these dolomitic fines by two types of pretreatments, hydration, and sonication, combined with different thermal conditions.

2. Materials and methods

2.1. Materials

The parent dolomite fines were supplied by INTOCAST Ibérica (Asturias, Spain) as a fine powder (<20 μm) obtained after the thermal sintering process (calcination). According to the analyses provided by the company, the material contains a Ca/Mg weight ratio of 2, mainly as oxides, with traces of Si, Fe and Al (total concentration < 0.5%). This material will be labelled as “D” in the manuscript, and identified as “fresh catalyst”.

This material was modified by different pretreatments, combining thermal (T), hydrothermal (W) and sonication (S) procedures. In case of the thermal pretreatment, the material was under flowing air (40 $mL{\cdot}min^{-1}$) rising the temperature up to 500 °C (“DT1”) and 800 °C (“DT2”), with a slope of 10 $°C{\cdot}min^{-1}$. The final temperature was held for 8 h.

The hydrothermal pretreatment consists of an initial hydration, suspending the material in water (100 $g{\cdot}L^{-1}$) at 80 °C for 4 h in a closed vessel. The water was then evaporated in a furnace at 85 °C overnight. The solid recovered was identified as “DW”. In a second step, this solid was thermally treated at 500 °C and 800 °C, accordingly to the procedure previously indicated, obtaining other two calcined materials labelled as “DWT1” and “DWT2”, respectively.

The first hydration step was also considered under sonication (using a Bandelin Sonorex instrument at 600 W under 20 kHz of frequency) for 4 h at room temperature (samples inside sealed vials to prevent air contact), obtaining the “DS” sample. After the corresponding drying and a thermal treatment at 500 and 800 °C, two calcined materials were obtained, identified as “DST1” and “DST2”.

2.2. Characterization

The thermal stability of D, DW and DS was studied by thermogravimetry in a TGA 55 (TA Instruments) using 10 mg of solid. The analyses were carried out in air (40 $mL{\cdot}min^{-1}$, 0.1 MPa) increasing the temperature up to 900 °C at 5 $°C{\cdot}min^{-1}$. A mass spectrometer (Pfeiffer Vacuum Omnistar Prisma) was coupled to analyse the exhausted gases.

The morphology of the samples was studied in a Micromeritic ASAP 2020 surface analyser by nitrogen physisorption using the Brunauer-Emmett-Teller (BET) approximation for the specific surface area and the Barrett-Joyner-Halenda (BJH) model for the total pore volume.

The concentration and strength distribution of acidic and basic sites was determined by temperature programmed desorption (TPD) analyses in an AutoChem 2920 TPD/TPR (Micromeritics) using NH_3 (2.5% mol in Ar) and CO_2 (99.9% mol) as probe molecules, respectively. The saturation phase was carried out for 1 h at room temperature, with 40 $mL{\cdot}min^{-1}$ of each gas. After removing the physisorbed molecules flowing He at room temperature (40 $mL{\cdot}min^{-1}$), the signals of NH_3 and CO_2 were followed by mass spectrometry while the temperature rises up to 900 °C at 5 $°C{\cdot}min^{-1}$. The crystalline structure of D, DW and DS was studied by XRD using a PANalytical X’Pert Pro powder diffractometer equipped with a Cu-K_α radiation source (λ = 0.154 nm) and a temperature-controlled chamber. Considering the expected phases, the analyses were done in a 2θ range of 27.5 – 43.5°, at a scanning rate of $0.26°{\cdot}s^{-1}$, whereas the temperature increases from 25 to 800 °C at 5 $°C{\cdot}min^{-1}$.

2.3. Carbon dioxide adsorption

CO_2 adsorption capacity was tested by thermogravimetry in the abovementioned apparatus for all the materials. Before the adsorption experiments, the corresponding sample was subjected to a surface cleaning treatment, flowing N_2 (40 $mL{\cdot}min^{-1}$) at 150 °C for 2 h. The adsorption curve was then obtained flowing 40 $mL{\cdot}min^{-1}$ of a pure CO_2 stream for 10 h, at 0.1 MPa and 25 °C. It should be noted that the scope is to determine adsorption capacities, since the design of adsorption-based processes requires a more detailed study of adsorption equilibrium and kinetics.

2.4. Acetone liquid-phase self-condensation

The acetone self-condensation was studied in a batch sealed stirred reactor of 500 mL (Autoclave Engineers EZE Seal), equipped with a PID temperature control and a pressure regulator. Reactions were carried out in absence of any solvent, using 150 mL of pure acetone (Sigma Aldrich, greater than 99.9%) and 3 g of catalyst in each batch. The reaction was pressurized with 20 bar of N_2 to prevent the acetone evaporation once reached the reaction temperature (120 °C). Samples were periodically collected to evaluate the evolution of the reaction with time. The identification of the different compounds involved was carried out by GC–MS (Shimadzu GC/MS QP 2010 Plus Instrument), whereas quantitative analyses were done in a GC-FID (Shimadzu GC-2010), using commercial samples to calibrate the signals. In both cases, a 30 m long TRB-5MS capillary column was used as the stationary phase.

The experimental data were analysed in terms of acetone conversion (x) and selectivities (S_i) and yields (φ_i) of the products, according to the

Equations 1–3, where "n_i" represents the number of carbons in the molecule, and "$C_{i,t}$" the concentration of any reaction product at a particular time. In all the cases, the carbon balance closure was higher than 99%, ensuring the representativeness of data reported.

$$Conversion: x(\%) = \left(1 - \frac{C_{ACE,t}}{C_{ACE,t0}}\right) \cdot 100 \quad (1)$$

$$Selectivity: S_i(\%) = \frac{n_i \cdot C_{i,t}}{\sum (n_i \cdot C_{i,t})} \cdot 100 \quad (2)$$

$$Yield: \varphi_i(\%) = \frac{n_i \cdot C_{i,t}}{n_{ACE} \cdot C_{ACE,t0}} \cdot 100 \quad (3)$$

3. Results and discussion

3.1. Materials characterization

Fig. 1 shows the thermogravimetric decomposition of the three uncalcined samples used in this work, the fresh one (D) as well as those after the hydrothermal (DW) and sonication (DS) pretreatments. The three materials demonstrate a similar decomposition sequence until the final obtention of the CaO.

A first decomposition region, from room temperature to 360 °C, corresponds to a loss of water weakly linked to the material. As it could be anticipated, this first mass loss is slightly more marked with DW and, mainly, DS materials, in good agreement with the hydration phase of their pretreatments. With this last material, two different slopes could be defined, the second and more marked one being congruent with a higher penetration in the structure because of the sonication.

A second step occurs in the temperature range 370–450 °C, with relative mass losses of 9.5, 10.7 and 12.9% for D, DW and DS, respectively. This loss corresponds to a large signal of H_2O, which suggests the decomposition of hydroxides, mainly $Ca(OH)_2$, obtained by hydration of the CaO phase. The weight loss is more pronounced for DW and DS since both pretreatments (in water) increase the initial $Ca(OH)_2$ concentration. The third step (540–680 °C) is accomplished by the release of CO_2, being associated with the decarbonation. This third step accounts mass losses for 8.5, 4.3 and 3.8% for D, DW and DS, respectively. In the cases of DW and DS materials, these relative decreases are lower than those observed in the second step, being justified by the high $Ca(OH)_2$/CaO surface ratio of pretreated samples. At temperatures over 680 °C, total stable profiles are observed in the three cases, corresponding with a stable structure of oxides. According to these results, 500 and 800 °C are the temperatures considered for the materials activation.

The hypotheses of the previous discussion were verified by the study of the evolution of the crystallographic phases with the temperature. These DRX analyses are shown in Fig. 2. As temperature increases, the diffraction peaks shift to the low angle, indicating a lattice expansion, being the common behaviour observed for most of the crystalline samples [Zhu et al., 2018; Hallam et al., 2021; Phillips et al., 2021]. Thus, signals at room temperature are used in the phase identification. Diffraction patterns demonstrate the prevalence of peaks related to CaO (lime) and MgO (periclase), with relevant contributions of $Ca(OH)_2$ (portlandite), with their main peaks at 37°, 43°, and 34°, respectively.

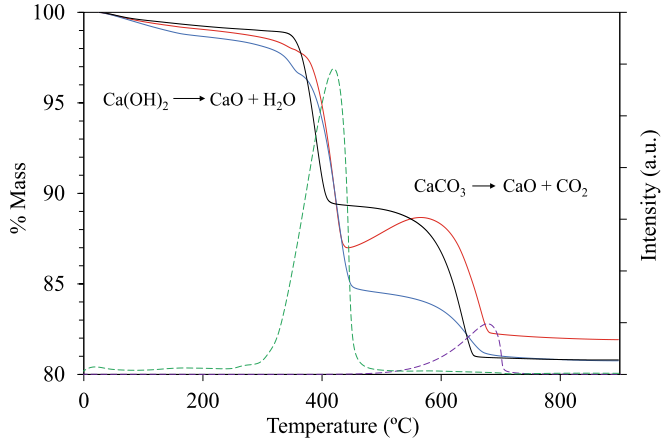

Fig. 1. Thermogravimetric decomposition curves obtained in air flow (40 mL·min^{-1}) for the different not-calcined materials. Curves corresponding to parent dolomite (D, black), hydrothermally treated (DW, red) and sonicated (DS, blue). Broken lines correspond to MS signals of water (green) and CO_2 (violet) detected in the released gases during the thermogravimetric decomposition of the parent dolomite (D).

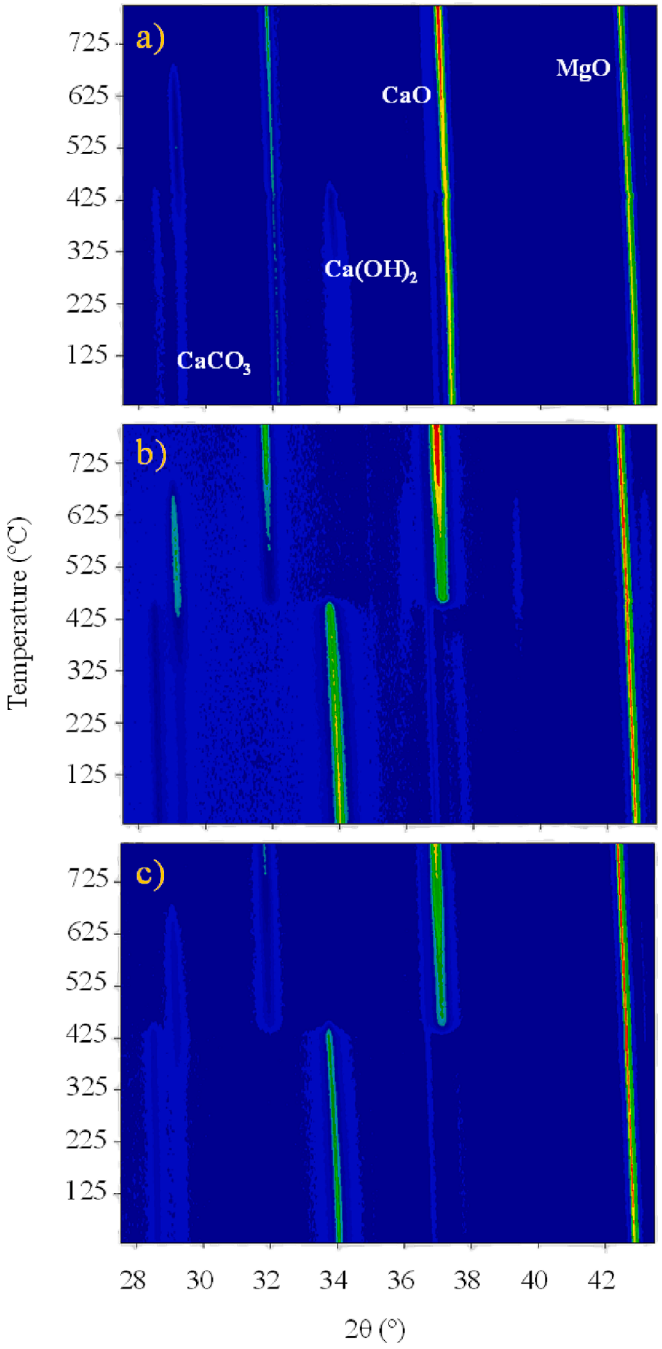

Fig. 2. XRD mapping of the 2θ range of 27.5–43.5° using a heating rate of 5 °C·min^{-1} between room temperature and 800 °C. Results corresponding to a) fresh sample (D); b) dolomite after hydrothermal treatment (DW); c) dolomite after sonication treatment (DS).

Intensity of $Ca(OH)_2$ peaks is significantly higher in DW and DS samples, due to the hydration pretreatment. In good agreement with the TG analyses, this phase disappears around 425 °C, with the subsequent enrichment in CaO, the main phase at high temperatures. In fact, with DW and DS samples, the appearance of peak at 37° takes place at the same temperature as the calcium hydroxide disappears. $CaCO_3$ is also detected in the three samples (2θ = 29°), but with low intensity, suggesting a high amorphous phase. In all the cases, these signals disappear before 680 °C, in good agreement with the last mass loss observed by TG.

In the case of the DW sample, the intensity of this phase increases from 425 to 650 °C, suggesting a recrystallization process before the $CaCO_3$ decomposition, a behaviour not observed with the fresh and sonicated samples. At this range, the thermogravimetric analysis in air atmosphere (Fig. 1) shows a mass gain shoulder, not observed with the other samples. This result has been previously reported for other dolomite samples [Lanas and Alvarez, 2004]. It should be mentioned that this shoulder does not appear if the thermogravimetry is made in nitrogen (**Fig. S1**), suggesting a key role of oxygen in this transformation.

The release of CO_2 by the oxidative decomposition of traces of siderite ($FeCO_3$) present in the material, and its capture by the CaO could be a theoretical explanation of this behaviour [Ponomar et al., 2017]. However, the weight gain is too high to be due to the low Fe concentration (<0.5 %), except if this Fe shows a catalytic behaviour. Moreover, there is not any reason to expect a surface exposition of Fe phases after the hydration pretreatment not observed after sonication, but this behaviour is not observed with the DS sample.

A second hypothesis suggests that the particular behaviour of DW sample can be explained attending to the structural oxygen vacancies generated during the crystallographic transformation from $Ca(OH)_2$ to CaO, releasing water. The relevance of these vacancies increases as the rate of this transformation increases, or the degree of order of the initial structure decreases [León et al., 2014]. It is suggested that the hydrothermal pretreatment promotes both effects, whereas the sonication contributes to a more ordered material. This hypothesis is in good agreement with the surface area values, as discussed below. These oxygen vacancies could induce oxygen preadsorption and activation on metal traces of the material and the formation of carbonates once the CO_2 from a stagnant layer over the solid could become part of the crystal structure [Solymosi 1991; Lanas and Alvarez 2004; Etim et al., 2021].

On the other hand, the lack of any signal at 30° discards the presence of dolomite phase ($Ca_{0.5}Mg_{0.5}CO_3$), concluding that, at room temperature, CO_2 is only absorbed on CaO phases, whereas the parent structure of the dolomite stone is not recovered.

The intensity of MgO peaks remains stable as temperature increases, result that supports the analysis of the mass loss based on the transformation of the phases related to calcium. However, the intensity of this signal is significantly higher once the material is pretreated. The surface exposition of MgO is one of the reported consequences of the dolomite pretreatments [Niu et al., 2014; Su et al., 2018]. The evolution of the relative MgO/CaO amount in these materials is analysed in **Fig. S2**, observing a constant ratio in the case of the fresh material (around 0.9). In the case of DW sample, this ratio is more than five times higher, suffering a fast decrease over 400 °C due to the appearance of new CaO phases. A similar but more marked behaviour is observed with DS sample, with initial MgO/CaO values slightly higher than 8. It is expected that these differences in the crystallinity affects to the catalytic and adsorption behaviour of these materials.

Based on these results, and trying to obtain solids with different properties, six materials were prepared by calcining the D, DW and DS solids at 500 and 800 °C (T1 and T2, respectively). The crystallographic structures of these materials are compared in **Fig. S3**.

Nitrogen adsorption isotherms for all the materials considered in this work are included in the supplementary information (**Fig. S4**), whereas the textural properties, as well as the main results of the basicity and acidity, are summarized in Table 1. All the materials show the expected adsorption behaviour obtained by a combination of types III and V-H3 isotherms, according to the IUPAC classification, suggesting that the different pretreatments do not alter the general surface properties of the parent material, being characterized by a slit-shaped porosity. This morphology is in good agreement with the previous literature for this type of materials [Avila et al., 2012].

A clear increase in the specific surface area is observed when the material undergoes hydrothermal and sonication pretreatments, suggesting that both techniques lead to surface expansion, being more marked in the case of hydrothermal samples, which agrees with the structural defects formed during the crystallographic transformation.

In all the cases, the calcination treatment at 500 °C increases the surface area, suggesting that the thermal decomposition of the $Ca(OH)_2$ produces not only the crystalline CaO but also some amorphous phases characterized by an increment in the porous volume and the presence of microporous. Both aspects justify the increase in the surface area observed. Thus, there is a total correspondence between total porous volume and mesoporous one in the case of the fresh dolomite (D, 0.0217 $cm^3 \cdot g^{-1}$), whereas DT1 and DWT1 and DST1 have a not inconsiderable volume of microporous (0.0014, 0.0011, and 0.0009,$cm^3 \cdot g^{-1}$, respectively). The comparative analysis after thermal treatment at 800 °C is not so clear, obtaining a significant decrease in the cases of DT2 and DST2 (in comparison with their corresponding fresh materials) but without observing any clear effect in the case of DWT2, material that presents the highest surface area. It is suggested that the thermal treatment at 800 °C, with the decomposition of all the carbonates, produces a reordering in the dolomite structure, justifying these decreases. As to the pore size, all the materials show a clear mesoporosity, with values from 13 to 32 nm. The hydrothermal and sonication pretreatments produce a decrease in the average size, with the corresponding increase in the pore volume. On the opposite, DWT1 is an exception to this general trend, being the material with the highest pore volume and the largest pores.

The significant effect of the pretreatments in the morphological parameters anticipate a relevant modification in their chemical properties, as it is demonstrated by the acidity and basicity tests. The desorption curves of all the materials are included in the Supplementary Information (**Fig. S5-S6**), whereas the main results are summarized in Table 1. All the samples demonstrate a significant increase in basicity, with

Table 1
Main morphological and chemical characterization results obtained by N_2 physisorption, CO_2-TPD and NH_3-TPD.

Material	Surface area ($m^2 \cdot g^{-1}$)	Average pore diameter (nm)	Pore volume ($cm^3 \cdot g^{-1}$)	Basicity		Acidity	
				(mmol $CO_2 \cdot g^{-1}$)	°C	(mmol $NH_3 \cdot g^{-1}$)	°C
D	3.5	19.8	0.021	0.112/0.145	641/693	0.333/0.553	402/425
DT1	9.1	19.3	0.076	0.924/0.509	735/768	0.272/1.367	354/434
DT2	3.3	32.1	0.047	0.092/0.159	592/644	0.062/0.221	340/383
DW	17.5	13.5	0.108	0.733/0.677	706/746	0.705/0.447	418/447
DWT1	27.1	22.8	0.171	0.732/0.653	697/740	0.399/0.165	395/413
DWT2	28.6	13.1	0.131	0.529/0.663	672/723	0.277/0.249	367/405
DS	12.3	19.3	0.083	0.335/0.141	619/655	0.215/0.279	405/431
DST1	22.2	14.1	0.114	0.811/0.554	707/747	0.420/0.736	377/417
DST2	9.9	17.2	0.101	1.460/0.636	705/749	0.209/0.168	357/394

respect to the fresh material, both in strength and concentration of the active sites. Thus, the concentration of basic sites with all the pretreated samples is more than five times higher than the initial 0.257 mmol $CO_2 \cdot g^{-1}$ of the parent dolomite fines, with the only exception of DT2, catalyst with the same basicity than the parent material. This catalyst is also the exception in the general strength trend since the pretreated catalyst show an average desorption temperature 50 °C higher than the desorption temperatures obtained with the parent material. The presence of stronger basic sites is congruent with the disappearance of hydroxides, and the prevalence of O^{2-} basic sites [Yanagisawa et al., 1995; León et al., 2011]. In all the cases, there is a clear correspondence between the increase in concentration and strength, DT1 and mainly DST2 being the most basic materials.

The softer desorption temperature of acidic sites is congruent with the presence of basic-acid pairs in which the medium-strength basic sites are associated to weaker acid ones. This has been deeply studied in the literature for similar oxides [Climent et al., 2010; Jensen et al., 2012]. In this case, the thermal treatment generally decreases the concentration of acidic sites, being more marked after calcination steps at 800 °C.

These differences in the basicity and acidity of the dolomite-derived catalyst are expected to have a relevant role in the behaviour of these materials in the two proposed processes: the CO_2 adsorption, and the acetone condensation, being possible to define the optimum pretreatment to each aim.

3.2. Carbon dioxide adsorption

The alkali nature of dolomite suggests is use as a suitable adsorbent for acid gases, such as CO_2. The adsorption mechanism based on the calcium looping process (CLP), a reversible carbonation reaction of CaO, is considered as the component with the major contribution to CO_2 adsorption in dolomites [Stendardo et al., 2011; Su et al., 2018]. The reaction fixes CO_2 to the CaO structure, obtaining the $CaCO_3$. The MgO is not considered as active for this adsorption because of kinetic reasons (very slow carbonation rate), although MgO plays a key role giving thermal stability and helping to mitigate the loss of CaO carbonation reactivity [Valverde et al., 2015].

The CO_2 adsorption was studied by thermogravimetry, at 25 °C and 0.1 MPa, the curves obtained being shown in Fig. 3. The almost null adsorption obtained with the untreated material (D) is congruent with its low surface area and its large $Ca(OH)_2$ and $CaCO_3$ concentrations. The thermal treatment of this sample increases its adsorption capacity, from 0.85 mg $CO_2 \cdot g^{-1}$ for D to 3.81 and 4.06 mg $CO_2 \cdot g^{-1}$ for DT1 and DT2, respectively. These values are congruent with the increase in basicity and surface area of these materials and demonstrate that the hygroscopic character of the parent dolomite fines prevails over the CO_2 chemisorption capacity since the highest increase is reached after the Ca $(OH)_2$ decomposition.

A low CO_2 adsorption capacity is also observed with DW (3.63 mg $CO_2 \cdot g^{-1}$). With this material, the positive effect of the relevant increase in the surface area is almost totally shielded by its high $Ca(OH)_2$ surface concentration. The CO_2 adsorption capacity is almost ten times higher with DWT1 (29.15 mg $CO_2 \cdot g^{-1}$). The reduction observed with DWT2 (16.35 mg $CO_2 \cdot g^{-1}$) is congruent with the reduction in basicity observed with this material, despite the high surface area of this solid.

As to sonicated materials, DS shows a CO_2 adsorption capacity of 8.18 mg $CO_2 \cdot g^{-1}$, whereas the DST1 demonstrates a CO_2 adsorption capacity (46 mg $CO_2 \cdot g^{-1}$) more than 50 times higher than with the parent DS. In this case, the curve suggests that exposition times higher than 10 h would be needed to reach the equilibrium. This value is the maximum obtained with the tested materials (at these conditions), its capacity being comparable with data reported for other materials, such as ZIF-95 (37.4 mg $CO_2 \cdot g^{-1}$) [Reddy et al., 2021], and slightly below Norit SX2 commercial activated carbon (63 mg $CO_2 \cdot g^{-1}$) [Rashidi et al., 2016] or activated sepiolite (65.1 mg $CO_2 \cdot g^{-1}$) [Tao et al, 2022].

These results suggest a general prevalence of basicity over surface

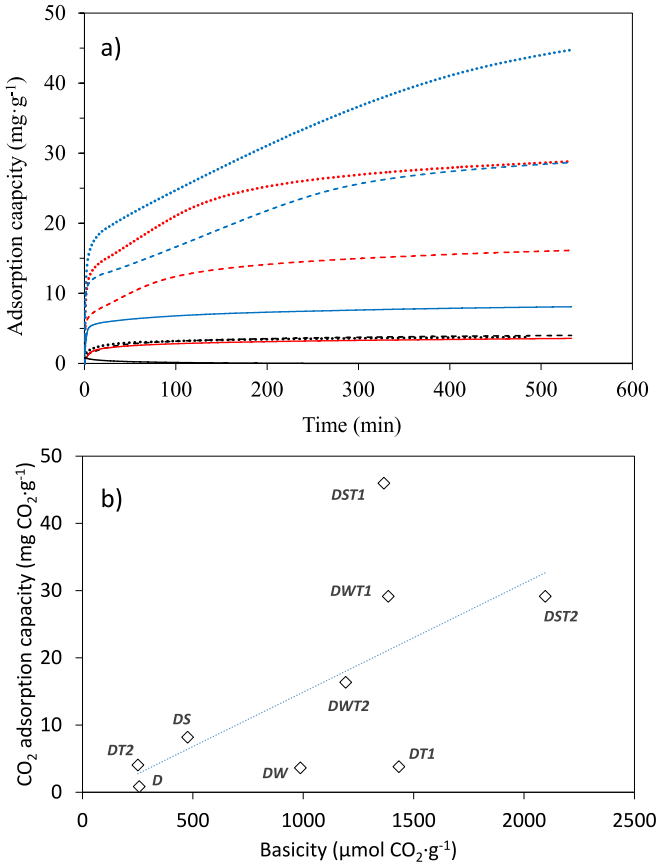

Fig. 3. A) pure co_2 adsorption curves obtained by thermogravimetry at 25 °C and 0.1 MPa. Grey lines indicate D-series materials (- D, ··· DT1,— DT2), orange lines indicate DW-series materials (-DW, · · ·DWT1, – – –DWT2), blue lines indicate DS-series materials (-DS, · · ·DST1, – – –DST2). DT1 and DT2 series are difficult to identify since they overlap; b) Correspondence between CO_2 adsorption capacity and the basicity of the different materials considered in this work.

area as the key parameter to increase the CO_2 adsorption capacity. The good correlation between these two parameters, mainly when comparing the materials obtained without calcination and after the thermal treatment at 800 °C, is shown in Fig. 3b.

A significant discrepancy is observed when considering the pretreated samples calcined at 500 °C. These results suggest that basic active sites of disordered CaO are the most active ones, the crystallinity of this phase being too high after the pretreatment at higher temperatures. Based on these experiments, the sonication pretreatment followed by calcination at 500 °C (DST1) is suggested as the optimum procedure to optimize this application of this by-product of the refractory industry.

3.3. Acetone liquid-phase self-condensation

Table 2 summarizes the main results obtained after 5 h of acetone self-condensation at 120 °C. In this table, the turnover frequency (TOF) value has been introduced to compare the activity of the different materials. This parameter is defined as the moles of acetone converted by mole of basic sites available (active sites for this reaction) and time. Significant differences between materials are observed, obtaining very low conversion with the fresh dolomite (D), 1.24 % after 5 h, but very promising results with the DST2, with more than 17.3 %. In general, the calcined catalysts (DT1, DT2, DWT1, DWT2, DST1 and DST2) are more active than their corresponding uncalcined counterparts (D, DW, and DS), the differences being more evident for samples treated at 500 °C. There is a clear correspondence between the acetone conversions and

Table 2
Summary of the main results obtained after 5 h of acetone (ACE) self-condensation in liquid phase at 120 °C as a function of the catalyst. Selectivities considering diacetone alcohol (DAA); mesityl oxide (MO), phorones (P), isophorones (IP), and mesitylene (M). TOF is calculated as moles of ACE converted by moles of basic sites and time.

Catalyst	ACE Conv (%)	Selectivity			Initial rate ($x10^{-5}$ $mol \cdot g^{-1} \cdot h^{-1}$)	TOF (h^{-1})
		DAA	MO	P + IP + M		
D	1.24	2.0	96.9	1.0	2.00	4.22
DT1	9.37	5.4	92.8	1.8	18.7	7.87
DT2	6.55	5.2	93.8	1.0	14.7	36.1
DW	3.32	4.7	94.6	0.8	8.00	3.86
DWT1	8.53	5.4	92.7	1.9	20.0	8.52
DWT2	9.68	5.9	93.5	0.5	23.3	11.5
DS	5.14	5.2	92.6	2.2	12.7	16.2
DST1	10.88	5.5	90.9	3.6	22.0	8.53
DST2	17.37	6.3	91.4	2.4	34.0	9.30

the total basicity of these materials, as illustrated in **Fig. S7**, without observing a preferential contribution of any specific strength. This apparent lack of requirements in strength is congruent with the products distribution, the reaction being almost totally limited to the first condensation steps.

Mesityl oxide is the main product observed, with selectivities higher than 90 % in all the cases, and<7 % of diacetone alcohol. These results corroborate a high dehydration capacity due to the presence of acid sites on these materials. There is a clear correspondence between the production of trimers (phorones, isophorones and, only in traces, mesitylene) with the strength of the basic sites of these materials. In any case, the reaction conditions are too soft to enhance this second condensation, with maximum selectivities lower than 4 % in all the cases. The requirement of strong basicity and higher temperatures to produce the second condensation, mainly in liquid phase, was previously discussed in the literature [Faba et al., 2013].

As shown in **Fig. S8**, the evolution of acetone conversion with reaction time suggests slight deactivation effects, probably due to the adsorption of the water release during the diacetone alcohol dehydration to obtain mesityl oxide [Ngo et al., 2018]. This adsorption modifies the activity of the basic sites, inhibiting the main reaction. The initial reaction rates were then evaluated considering the first two hours of reaction, to minimize the effects of catalyst deactivation. There is not agreement in the literature about the kinetic order of the acetone self-condensation, with authors proposing a first-order model (considering the limiting step the enolization of one of the acetone molecules involved) [Faba et al., 2013; Herrmann et al., 2017] and other authors suggesting a second order, in which both molecules are involved [Talwalkar and Mahajani 2006]. The fit considering both models is compared in **Fig. S9**, including the kinetic rates and the regression coefficients in Table S1. Good fits were obtained with both models, being slightly better those considering the bimolecular model. Thus, the second order mechanism is proposed for these materials, these kinetic rates being the ones chosen to calculate the TOF values shown in Table 2.

Experimental results were fitted to different bimolecular models, the best results being obtained with the bimolecular single site Eley-Rideal one (a model previously proposed in the literature for this reaction) [Li et al., 2020] considering inhibition due to water adsorption on these active sites [Talwalkar and Mahajani 2006], according to Eq. (4):

$$\frac{d[ACE]}{dt} = -\frac{k \cdot K_{EN} \cdot K_{ads} \cdot [ACE]^2}{1 + K_{ads} \cdot [ACE] + K_{water} \cdot [H_2O] + K_{ads} \cdot K_{EN} \cdot [ACE]} \quad (4)$$

In this model, "k" is the kinetic rate, "K_{EN}" corresponds to the equilibrium constant for enolization, and "K_{ads}" and "K_{water}" are the two adsorption constants considered, the acetone and water one, respectively. Considering the products distribution, there is a direct correspondence between the MO produced and the water released since the relevance of phorones and isophorones (the other compounds whose production releases water) is negligible. Thus, the kinetic equation can be modified to Eq. (5):

$$\frac{d[ACE]}{dt} = -\frac{k \cdot K_{EN} \cdot K_{ads} \cdot [ACE]^2}{1 + K_{ads} \cdot (1 + K_{EN})[ACE] + K_{water} \cdot [MO]} \quad (5)$$

In the fitting of the data, the equilibrium constant of enol formation (K_{EN}) was restricted to be the same for all the materials since it is a thermodynamics parameter, while the rate and adsorption constants were allowed to vary for each catalyst. Table 3 summarizes all the constants obtained with the different catalysts, whereas the goodness of this model is illustrated in Fig. 4, where the experimental evolutions of acetone and mesityl oxide are compared with the fitted values obtained with the kinetic adjustment.

As shown in Table 3, the proposed model fairly predicts the experimental results, obtaining appropriate regression coefficients (higher than 0.99 in all the cases). The value of the equilibrium constant of enol formation (K_{EN}) is higher than the value proposed in the literature (0.535) [Li et al., 2020]. This result is explained by the different temperatures used in both studies (120 °C in this work, and 200 °C in the previous study [Li et al., 2020]), considering the endothermic character of the enolization [Malhotra et al., 2017].

The values of the adsorption constants do not show clear correlation with the surface area or the basicity, suggesting that both adsorption steps are specific processes conditioned by the chemical structure of the surface and not directly to morphological parameters. Values obtained for water adsorption are significantly higher than those for the acetone one, justifying the temporal profiles observed with all the materials. The minimum value for this adsorption is obtained with the fresh sample (D), as expected because of its carbonate structure, whereas the influence of this adsorption increases once the sample is calcined (after obtaining the corresponding oxides). On the contrary, the pretreated but uncalcined materials (DW and DS) show significantly higher water adsorption values than the one obtained with D sample, in agreement with the increase in the surface area, the exposition of more anchoring points after the pretreatment, and the absence of carbonates on the surface. Once these materials suffer the thermal treatment, the K_{water} decreases. This could be explained by the increase in the crystallinity of these materials, as discussed in the characterization results (XRD, Fig. S3).

There is a clear correlation of the kinetic rates with the basicity of these materials, as shown in Fig. 5, demonstrating that this property conditions the catalytic activity, whereas the differences in surface area or acidity are not significative. In the same way, a common evolution is observed, without any difference due to the type of pretreatment applied to the dolomite fines.

To sum up, the best catalytic results are obtained with DST2, with 17.4 % of acetone conversion in<5 h, obtaining mesityl oxide with a selectivity higher than 91 % which corresponds to yields of 17 %. This approach is not considered in the literature since most of the works

Table 3
Optimized parameters obtained applying the proposed kinetic model for the acetone self-condensation at 120 °C with the different dolomite-derived materials considered in this work.

Catalyst	k ($L \cdot mol^{-1} \cdot s^{-1}$)	K_{ads} ($L \cdot mol^{-1}$)	K_{water}($L \cdot mol^{-1}$)	K_{EN}	r^2
D	$2.8 \cdot 10^{-6}$	0.08	44.5	1.233	0.942
DT1	$1.9 \cdot 10^{-4}$	0.07	82.7		0.998
DT2	$5.9 \cdot 10^{-5}$	0.22	348.4		0.9998
DW	$1.6 \cdot 10^{-4}$	0.06	121.3		0.9999
DWT1	$1.3 \cdot 10^{-4}$	0.14	104.5		0.9993
DWT2	$1.7 \cdot 10^{-4}$	0.08	61.9		0.9997
DS	$1.2 \cdot 10^{-4}$	0.05	116.7		0.9998
DST1	$2.1 \cdot 10^{-4}$	0.22	66.3		0.9996
DST2	$3.0 \cdot 10^{-4}$	0.19	52.3		0.998

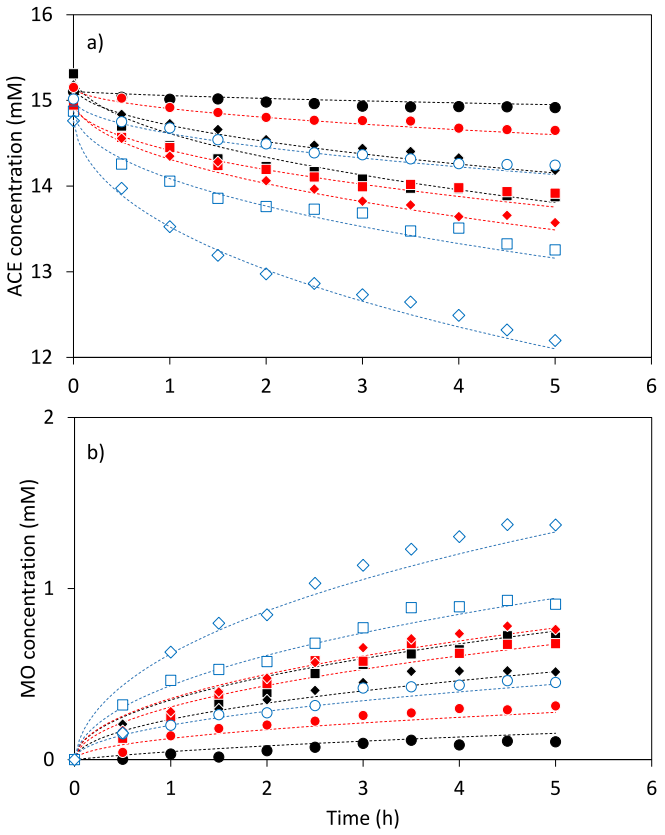

Fig. 4. Evolution of (a) acetone and (b) mesityl oxide at 120 °C as a function of the catalyst. Experimental points: (●) D, (■) DT1, (◆) DT2, (●) DW, (■) DWT1, (◆) DWT2, (○) DS, (□) DST1, (◇) DST2. Broken lines correspond to the fitted values according to the proposed kinetic model.

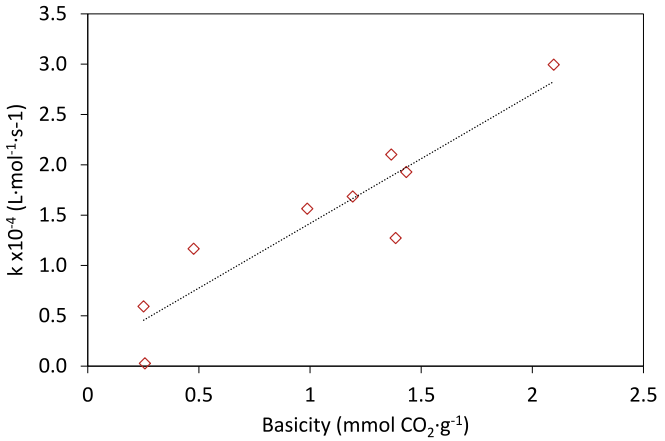

Fig. 5. Correlation between the kinetic rate constant and the basicity of the different catalysts tested in this work.

produce significant amounts of mesityl oxide when working in gas-phase, the isophorones and mesitylene being the main products [Toit and Nicol 2004; O'Keefe et al., 2010]. As to previous studies in liquid-phase, most of them are focused on maximizing the diacetone alcohol, obtaining the mesityl oxide as a secondary product [Tichit et al, 1998; Houssaini et al., 2021]. These results demonstrate that pretreated dolomite fines (a by-product of refractory materials manufacturing) can be considered as a promising catalyst for the selective acetone liquid-phase condensation to produce mesityl oxide, a relevant solvent for synthetic fibres, oils, resins, and inks.

4. Conclusions

Physical pretreatments (hydrothermal and, mainly, sonication) combined with thermal activation are demonstrated to be good procedures to activate dolomite fines (a low-cost by-product of the refractory materials manufacturing), obtaining interesting materials with promising applications as CO_2 adsorbents and, mainly basic catalyst for the acetone liquid-phase self-condensation. A complete characterization clearly shows the positive effect of these pretreatments in the basicity and surface area, as well as a higher surface exposition of MgO phases.

As adsorbent, the best results are obtained with the sample after sonication and thermal activation at 500 °C (DST1), with a CO_2 adsorption capacity of 46 $mg \cdot g^{-1}$, this value being two times higher than the expected one considering its basicity. This result demonstrates the goodness of sonication treatment to expose more anchoring points on the surface.

Sonication is also highlighted as the best pretreatment to enhance the catalytic activity in the acetone condensation, obtaining 17 % of conversion (reaction in absence of external solvent) after 5 h at 120 °C, with more than 90 % of mesityl oxide selectivity. A comprehensive kinetic analysis of experimental results demonstrates the proportionality between activity and basicity, and the relevant role of adsorption processes on the catalytic activity and deactivation.

Declaration of Competing Interest

The authors declare that they have no known competing financial interests or personal relationships that could have appeared to influence the work reported in this paper.

Data availability

Data will be made available on request.

Acknowledgments

This work was supported by INTOCAST Ibérica and by the Asturian Government (contract GRUPIN AYUD/2021/50450). The authors acknowledge the technical support provided by *Servicios Científico-Técnicos* from Universidad de Oviedo (XRD data collection and interpretation).

Appendix A. Supplementary material

Supplementary data to this article can be found online at https://doi.org/10.1016/j.wasman.2023.06.031.

References

Aksel'rod, L.M., Kvyatkovskii, O.V., New technology, new refractories. Engineering-economic analysis, Refractor. Ind. Ceram. 44 (2003) 32-36. https://doi.org/10.1023/A:1023915728034.

Al-Hazmi, M.H., Choi, Y.M., Apblett, A.W., 2013. Acetone condensation over sulphated zirconia catalysts. Catal. Lett. 143, 705–716. https://doi.org/10.1007/s10562-013-1020-8.

Ávila, I., Crnkovic, P.M., Milioli, F.E., Luo, K.H., 2012. Investigation of the pore blockage of a Brazilian dolomite during the sulfation reaction. Appl. Surf. Sci. 258, 3532–3539. https://doi.org/10.1016/j.apsusc.2011.11.108.

Climent, M.J., Corma, A., De Frutos, P., Iborra, S., Noy, M., Velty, A., Concepción, P., Chemicals from biomass: synthesis of glycerol carbonate by transesterification and carbonylation with urea with hydrotalcite catalysts. The role of acid-base pairs, J. Catal. 269 (2010) 140-149, https://doi.org/100.1016/j.jcat.2009.11.001.

Deneen, M.A., Gross, A.C., 2010. Refractory materials: the global market, the global industry. Bus. Econ. 45, 288–295. https://doi.org/10.1057/be.2010.30.

Deng, J.M., Liu, J., Li, S., Dewil, R., Zhang, H.L., Baeyens, J., Mikulcic, H., 2022. The steam-assisted calcination of limestone and dolomite for energy savings and to foster solar calcination processes. J. Clean Prod. 363, 132640 https://doi.org/10.1016/j.clepro.2022.132640.

du Toit, E., Nicol, W., 2004. The rate inhibiting effect of water as a product on reactions catalysed by cation exchange resins: formation of mesityl oxide from acetone as case study. Appl. Catal. A 277, 219–225. https://doi.org/10.1016/j.apcata.2004.09.015.
Duchesne, J., Reardon, E.J., 1999. Lime treatment of fly ash: characterization of leachate composition and solid/water reactions. Waste Manag. 19, 221–231. https://doi.org/10.1016/S0956-053X(99)00052-5.
Efremenkov, V.V., 2016. Design particularites of dolomite processing lines for glass batch production. Glas. Ceram. 73, 175–179. https://doi.org/10.1007/s10717-016-9850-7.
Etim, U.J., Zhang, C., Zhong, Z., 2021. Impacts of the catalyst structures on CO_2 activation on catalyst surfaces. Nanomaterials 11, 3265. https://doi.org/10.3390/nano11123265.
Faba, L., Díaz, E., Ordóñez, S., 2013. Gas phase acetone self-condensation over unsupported and supported MgZr- mixed oxides catalysts. Appl. Catal. B 142, 387–395. https://doi.org/10.1016/j.apcatb.2013.05.043.
Faba, L., Gancedo, J., Quesada, J., Díaz, E., Ordóñez, S., 2021. One-pot conversión of acetone into mesitylene over combinations of acid and basic catalysts. ACS Catal. 11, 11650–11662. https://doi.org/10.1021/acscatal.1c03095.
Furlani, E., Rondienella, A., Aneggi, E., Maschio, S., 2021. Possible recycling of end-of-life dolomite refractories by the production of geopolymer-based composites: experimental investigation. J. Sustain. Metall. 7, 908–919. https://doi.org/10.1007/s40831-021-00383-x.
Ghaemi, A., Torab-Mostaedi, M., Ghannadi-Maragheh, M., 2011. Characterizations of strontium (II) and barium (II) adsorption from aqueous solutions using dolomite powder. J. Hazard. Mater. 190, 916–921. https://doi.org/10.1016/j.jhazmat.2011.04.006.
Ghaemi, A., Torab-Mostaedi, M., Shahhosseini, S., Asadollahzadeh, M., 2013. Characterization of Ag(I), Co(II) and Cu(II) removal process from aqueous solutions using dolomite powder. Korean J. Chem. Eng. 30, 172–180. https://doi.org/10.1007/s11814-012-1113-1.
Ghosh, A., Tripathi, H.S., 2012. Sintering behaviour and hydration resistance of reactive dolomite. Ceramics Int. 38, 1315–1318. https://doi.org/10.1016/j.ceramint.2011.09.005.
Hafriz, R.S.R.M., Shafizah, I.N., Arifin, N.A., Salmiaton, A., Yunus, R., Yap, Y.H.T., Shamsuddin, A.H., 2021. Effect of Ni/Malaysian dolomite catalyst synthesis technique on deoxygenation reaction activity of waste cooking oil, Renew. Energ. 178, 128–143. https://doi.org/10.1016/j.renene.2021.06.074.
Hallam, K.R., Darnbrough, J.E., Paraskevoulakos, C., Heard, P.J., Marrow, T.J., Flewitt, P.E.J., 2021. Measurements by x-ray diffraction of the temperature dependence of lattice parameter and crystallite size for isostatically-pressed graphite. Carbon Trends 4, 100071. https://doi.org/10.1016/j.cartre.2021.100071.
Herrmann, S., Iglesia, E., 2017. Elementary steps in acetone condensation reactions catalyzed by aluminosilicates with diverse void structures. J. Catal. 346, 134–153. https://doi.org/10.1016/j.jcat.2016.12.011.
Houssaini, J., Bennani, M.N., Ziyat, H., Arhzaf, S., Qabaqous, O., Amhoud, A., 2021. Study of the catalytic activity of the compounds hydrotalcite type treated by microwave in the self-condensation of acetone. Int. J. Anal. Chem. 2021, 1551586. https://doi.org/10.1155/2021/1551586.
Huang, H., Zhang, D., Guo, G., Jian, Y., Wang, M., Zhang, P., Li, J., 2018. Dolomite application for the removal of nutrients from synthetic swine wastewater by a novel combined electrochemical process. Chem. Eng. J. 335, 665–675. https://doi.org/10.1016/j.cej.2017.11.013.
Industry Research Biz, Global methyl isobutyl ketone (MIBK) industry research report, growth trends and competitive analysis 2022-2028. https://www.industryresearch.biz/purchase/21758938.
Islam, M.W., 2020. A review of dolomite catalyst for biomass gasification tar removal. Fuel 267, 117095. https://doi.org/10.1016/j.fuel.2020.117095.
Jensen, M.B., Morandi, S., Prinetto, F., Sjastad, A.O., Olsbye, U., Ghiotti, G., 2012. FT-IR characterization of supported Ni-catalysts: influence of different supports on the metal phase properties. Catal. Today 197, 38–49. https://doi.org/10.1016/j.cattod.2012.06.016.
Karaca, S., Gürses, A., Ejder, M., Acikyildiz, M., 2006. Adsorptive removal of phosphate from aqueous solutions using raw and calcinated dolomite. J. Hazard. Mater. 128, 273–279. https://doi.org/10.1016/j.jhazmat.2005.08.003.
Korkut, I., Bayramoglu, M., 2016. Ultrasound assisted biodiesel production in presence of dolomite catalyst. Fuel 180, 624–629. https://doi.org/10.1016/j.fuel.2016.04.101.
Lanas, L., Alvarez, J.I., 2004. Dolomite limes: evolution of the slaking process under different conditions. Thermochim. Acta 423, 1–12. https://doi.org/10.1016/j.tca.2004.04.016.
León, M., Díaz, E., Vega, A., Ordóñez, S., Auroux, A., 2011. Consequences of the iron-aluminium exchange on the performance of hydrotalcite-derived mixed oxides for ethanol condensation. Appl. Catal. B 102, 590–599. https://doi.org/10.1016/j.apcatab.2010.12.044.
León, M., Faba, L., Díaz, E., Bennici, S., Ordóñez, S., Auroux, A., 2014. Consequences of MgO activation procedures on its catalytic performance for acetone self-condensation. Appl. Catal. B 147, 796–804. https://doi.org/10.1016/j.apcatb.2013.10.014.
Li, G., Ngo, D.T., Yan, Y., Tan, Q., Wang, B., Resasco, D.E., 2020. Factors determining selectivity of acid- and base-catalyzed self- and cross-condensation of acetone and cyclopentanone. ACS Catal. 10, 12790–12800. https://doi.org/10.1021/acscatal.0c02987.
Malhotra, S., Jaspal, D., Khamparia, S., 2017. p-Chloroacetophenone: a study of enolization kinetics. Chem. Eng. Commun. 204, 1445–1451. https://doi.org/10.1080/00986445.2017.1367672.
Manriquez-Ramirez, M.E., Elizalde, I., Ortiz-Islas, E., 2020. Synthesis of MgO and MgO-CeO(2) by co-precipitation for the catalytic conversion of acetone by aldol condensation. React. Kinet. Mech. Cat. 131, 769–780. https://doi.org/10.1007/s11144-020-01868-8.
Meng, D., Zhang, Y., Wang, Z., Qu, X., Gao, J., Jiao, T., Liang, P., 2019. Study on sulphur conversion characteristics in catalytic cracking of coal tar in the presence of dolomite-supported catalysts. Energy Fuels 33, 5102–5109. https://doi.org/10.1021/acs.energyfuels.9b00832.
Muñoz, I., Soto, A., Maza, D., Bayón, F., 2020. Life cycle assessment of refractory waste management in a Spanish steel works. Waste Manag. 111, 1–9. https://doi.org/10.1016/j.wasman.2020.05.023.
Ngo, D.T., Sooknoi, T., Resasco, D.E., 2018. Improving stability of cyclopentanone aldol condensation MgO-based catalysts by surface hydrophobization with organosilanes. Appl. Catal. B 237, 835–843. https://doi.org/10.1016/j.apcatab.2018.06.044.
Niu, S.-L., Huo, M.-J., Lu, C.-M., Liu, M.-Q., Li, H., 2014. An investigation on the catalytic capacity of dolomite in transesterification and the calculation of kinetic parameters. Bioresour. Technol. 158, 74–80. https://doi.org/10.1016/j.biortech.2014.01.123.
O'Keefe, W.K., Ng, F.T.T., Rempel, G.L., 2010. Kinetics of the syntheses of mesityl oxide (MO) and methyl isobutyl ketone (MIBK) in a fixed-bed flow reactor (FBR). Topic. Catal. 53, 1104–1109. https://doi.org/10.1007/s11244-010-9541-5.
Pehlivan, E., Ozkan, A.M., Dinc, S., Parlayici, S., 2009. Adsorption of Cu^{2+} and Pb^{2+} ion on dolomite powder. J. Hazard. Mater. 167, 1044–1049. https://doi.org/10.1016/j.jhazmat.2009.01.096.
Phillips, R., Jolley, K., Zhou, Y., Smith, R., 2021. Influence of temperature and point defects on the X-ray diffraction patterns of graphite. Carbon Trends 5, 100124. https://doi.org/10.1016/j.cartre.2021.100124.
Ponomar, V.P., Dudchenko, N.O., Brik, A.B., 2017. Phase transformations of siderite ore by the thermomagnetic analysis data. J. Magn. Magn. Mater 423, 373–378. https://doi.org/10.1016/j.jmmm.2016.09.124.
Qi, Z., Zhang, L., Jiang, F., Li, Y., Cang, D., Jin, H., Wang, C., Wu, W., Quian, W., Mukiza, E., 2019. New insight into the modification of pore structure in porous ceramics prepared from fly ash rich in CaO. Chemistry Select 4, 13884–13891. https://doi.org/10.1002/slct.201904130.
Rapagna, S., Gallucci, K., Foscolo, P.U., 2018. Olivine, dolomite and ceramic filters in one vessel to produce clean gas from biomass. Waste Manag. 71, 792–800. https://doi.og/10.1016/j.wasman.2017.07.038.
Rashidi, N.A., Suzana, Y., Borhan, A., 2016. Isotherm and thermodynamics analysis of carbon dioxide on activated carbon. Proced. Eng. 148, 630–637. https://doi.org/10.1016/j.proeng.2016.06.527.
Reddy, M.M.B., Ponnamma, D., Sadasivuni, K.K., Kumar, B., Abdullah, A.M., 2021. Carbon dioxide adsorption based on porous materials. RSC Adv. 11, 12658–12681. https://doi.org/10.1039/D0RA10902A.
Seifert, S., Dittrich, S., Bach, J., 2021. Recovery of raw materials from ceramic waste materials for the refractory industry. Processes 9, 228–244. https://doi.org/10.3390/pr9020228.
Serafin, J., Ouzzine, M., Cruz, O.F., Srenscek-Nazzal, J., Gomez, I.C., Azar, F.Z., Mafull, C.A.R., Hotza, D., Rambo, C.R., 2021. Conversion of fruit waste-derived biomass to highly microcoporous activated carbon for enhanced CO2 capture. Waste Manag. 136, 273–282. https://doi.org/10.1016/j.wasman.2021.10.025.
Solymosi, F., 1991. The bonding, structure and reactions of CO_2 adsorbed on clean and promoted metal surfaces. J. Molec. Catal. 65, 337–358. https://doi.org/10.1016/0304-5102(91)85070-I.
Stendardo, S., Di Felice, L., Gallucci, K., Foscolo, P.U., 2011. CO_2 capture with calcined dolomite: the effect of sorbent partice size. Biomass Conv. Bioref. 1, 149. https://doi.org/10.1007/s13399-011-0018-y.
Sun, J., Yang, Y., Guo, Y., Xu, Y., Li, W., Zhao, C., Liu, W., Lu, P., 2018. Stabilized CO_2 capture performance of wet mechanically activated dolomite. Fuel 222, 334–342. https://doi.org/10.1016/j.fuel.2018.02.162.
Talwalkar, S., Mahajani, S., 2006. Synthesis of methyl isobutyl ketone from acetone over metal-doped ion exchange resin catalyst. Appl. Catal. A 302, 140–148. https://doi.org/10.1016/j.apcata.2006.01.004.
Tamaddon, F., Tayefi, M., Hosseini, E., Zare, E., 2013. Dolomite ($CaMg(CO_3)_2$) as a recyclable natural catalyst in Henry, Knoevenagel, and Michael reactions. J. Molec. Catal. A 366, 36–42. https://doi.org/10.1016/j.molcata.2012.08.027.
Tao, H., Quian, X., Zhou, Y., Cheng, H., 2022. Research progress of clay minerals in carbon dioxide capture. Renew. Sust. Energ. Rev. 164, 112536 https://doi.org/10.1016/j.rser.2022.112536.
Tian, Q., Guo, B., Nakama, S., Zhang, L., Hu, Z., Sasaki, K., 2019. Reduction of undesirable element leaching from fly ash by adding hydroxylated calcined dolomite. Waste Manag. 86, 23–35. https://doi.org/10.1016/wasman.2019.01.027.
Tichit, D., Bennani, M.N., Figueras, F., Tessier, R., Kervennal, J., 1998. Aldol condensation of acetone over layered double hydroxides of the meixnerite type. Appl. Clay Sci. 13, 401–415. https://doi.org/10.1016/S0169-1317(98)00035-0.
Umadevi, T., Nelson, K., Mahapatra, P.C., 2009. Influence of magnesia on iron ore sinter properties and productivity. Ironmak Steelmak 36, 515–520. https://doi.org/10.1179/174328109X445741.
Valverde, J.M., Sanchez-Jimenez, P.E., Perez-Maqueda, L.A., 2015. Ca-looping for postcombustion CO_2 capture: a comparative analysis on the performances of dolomite and limestone. Appl. Energ. 138, 202–215. https://doi.org/10.1016/j.apenergy.2014.10.087.
Wang, K., Yin, Z., Zhao, P., Han, D., Hu, X., Zhang, G., 2015. Effect of chemical and physical treatments on the properties of a dolomite used in Ca looping. Energy Fuel 29, 4428–4435. https://doi.org/10.1021/acs.energyfuels.5b00853.
Yan, S., Wang, Q., Liu, J., Huo, W., Yang, J., Huang, Y., 2019. Synthesis, characterization and adsorption properties of low-cost porous calcined dolomite microspheres for removal of dyes. J. Wuhan, Univ. Technol. 34, 507–515. https://doi.org/10.1007/s11595-019-2080-4.

Yanagisawa, Y., Takaoka, K., Yamabe, S., Ito, T., 1995. Interaction of CO_2 with magnesium oxide surfaces: a TPD, FTIR, and cluster-model calculation study. J. Phys. Chem. 99, 3704–3710. https://doi.org/10.1021/j100011a043.

Yang, H., Dong, H., Zhang, T., Zhang, Q., Zhang, G., Wang, P., Liu, Q., 2019a. Calcined dolomite: an efficient and recyclable catalyst for synthesis of α, β-unsaturated carbonyl compounds. Catal. Letters 149, 778–1187. https://doi.org/10.1007/s10562-018-2632-9.

Yang, X., Li, Y., Ma, X., Zhao, J., Wang, Z., Liu, H., 2019b. CO_2 capture by a novel CaO/MgO sorbent fabricated from industrial waste and dolomite at calcium looping conditions. New J. Chem. 43, 5116–5125. https://doi.org/10.1039/C8NJ06257A.

Zhu, L.F., Liu, Q., Zhang, B.P., Cen, Z.-Y., Wang, K., Li, J.J., Bai, Y., Wang, X.H., Li, J.F., 2018. Temperature independence of the piezoelectric properties for high-performance $BiFFeO_3$-$BaTiO_3$ lead-free piezoelectric ceramics up to 300°C. RSC Adv. 62, 35794–35801. https://doi.org/10.1039/C8RA07553K.